Understanding the spectra of a few electrons confined in a quasi-one-dimensional nanostructure

2008 J. Phys.: Condens. Matter 20 155202

(http://iopscience.iop.org/0953-8984/20/15/155202)

J. Phys.: Condens. Matter **20** (2008) 155202 (13pp) doi:10.1088/0953-8984/20/15/155202

Understanding the spectra of a few electrons confined in a quasi-one-dimensional nanostructure

Tokuei Sako[1] **and Geerd H F Diercksen**[2]

[1] Laboratory of Physics, College of Science and Technology, Nihon University, 7-24-1 Narashinodai, Funabashi, 274-8501 Chiba, Japan
[2] Max-Planck-Institut für Astrophysik, Karl-Schwarzschild-Strasse 1, D-85741 Garching, Germany

E-mail: sako@phys.ge.cst.nihon-u.ac.jp and ghd@mpa-garching.mpg.de

Received 9 December 2007, in final form 21 February 2008
Published 25 March 2008
Online at stacks.iop.org/JPhysCM/20/155202

Abstract

The energy spectra and wavefunctions of three electrons confined by a quasi-one-dimensional Gaussian potential have been calculated and analyzed for three regimes of the strength of confinement ω_z, namely large ($\omega_z = 5.0$), medium ($\omega_z = 1.0$) and small ($\omega_z = 0.1$), by using the full configuration interaction method. For large and medium ω_z the energy spectrum shows a band structure which is characterized by the polyad quantum number v_p, while for small ω_z it is characterized by the extended polyad quantum number v_p^*. The wavefunctions of the quartet states have been assigned uniquely by counting the number of *nodal planes* for the three normal modes, namely, the center-of-mass, permutation and breathing modes. The energy levels for small ω_z form nearly degenerate triplets, each of which consists of two doublet states and one quartet state. The nodal patterns of their wavefunctions in this small ω_z regime are almost identical to each other except for their phases. The origin of the tripling of energy levels and the similarity of the wavefunctions for different spin states has been rationalized by using the projection of one- and two-electron potentials onto the *internal plane*. Effects of anharmonicity in the confining potential on the energy spectra and wavefunctions have also been examined.

(Some figures in this article are in colour only in the electronic version)

1. Introduction

Electrons confined in engineered low-dimensional nanospaces, referred to as quantum dots or artificial atoms [1–4], are known to have potential applicability to lasers [5, 6] and quantum computers [7, 8], since their electronic properties can be controlled by the size of the dots [9], their shape [10, 11] and their dimensionality [12, 13]. It has been demonstrated computationally that the energy-level structure of quantum dots changes strongly for different strengths of confinement [14, 15, 4, 16–18]. This is caused by a strong variation of the contribution of electron–electron interaction to the total energy with respect to the strength of confinement [4]. For the strong limit the confining potential dominates the energy spectrum and the electron–electron interaction plays only a minor role. For the weak limit of confinement, on the other hand, the electron–electron interaction becomes so large that it breaks the shell structure resulting from the confining potential [19, 18] and gives rise to a new structure in the energy spectrum as a result of Wigner crystallization [20].

In a previous study of this series [21], quantum dots have been modeled by two interacting electrons confined in a quasi-one-dimensional Gaussian potential [22, 23], and a detailed analysis has been made of the wavefunctions in order to clarify the relation between the form of the confining potential and the resulting energy spectra and dynamics of the electrons inside the dots. It has been shown in the study that the variation of the energy spectrum for different strengths of confinement can be understood in a unified way by counting the number of nodes in the wavefunction for each state. It has been also shown that *anharmonicity* in the Gaussian potential introduces irregularities in the energy spectrum and that the

wavefunctions of the corresponding states indicate localized motion of electrons [21]. On the other hand, two-electron quantum systems are not general multi-electron systems since the orbital and spin parts of their wavefunctions are separated from each other, and since after separating the center-of-mass degree of freedom the number of internal degrees of freedom of the electrons is limited to only one. Therefore, systems with more than two electrons have to be studied in order to understand the general trends in the energy spectrum of multi-electrons confined in quasi-one-dimensional potential walls.

In the present study, aiming at the general understanding of the energy spectrum and the dynamics of electrons of multi-electron quantum dots, a detailed analysis has been made of the system of three electrons confined in a quasi-one-dimensional Gaussian potential in which the spatial and orbital parts of the wavefunction are no longer separable and the number of internal degrees of freedom is more than one. The eigenvalues and wavefunctions of the three electrons have been calculated by using the quantum chemical full configuration interaction method employing a Cartesian anisotropic Gaussian basis set with high angular momentum functions [24]. The three-electron wavefunctions have been plotted in a three-dimensional space and their nodal patterns have been analyzed and used to interpret the energy spectra. Atomic units are used throughout this paper.

2. Computational methodology

The Hamiltonian operator adopted in the present study is a direct extension of the previous model [21] to the multi-electron case, namely,

$$\mathcal{H} = \sum_{i=1}^{N}\left[-\frac{1}{2}\nabla_i^2\right] + \sum_{i=1}^{N} w(\boldsymbol{r}_i) + \sum_{i>j}^{N}\frac{1}{|\boldsymbol{r}_i - \boldsymbol{r}_j|}, \qquad (1)$$

where N denotes the number of electrons. The one-electron confining potential $w(\boldsymbol{r})$ is the sum of an isotropic harmonic-oscillator potential for the x and y directions and an attractive Gaussian-type potential for the z direction and is given by

$$w(\boldsymbol{r}) = \frac{1}{2}\omega_{xy}^2\left[x^2 + y^2\right] - D\exp\left[-\frac{\omega_z^2}{2D}z^2\right]. \qquad (2)$$

For a sufficiently large value of ω_{xy} the electrons bound by the potential (2) are strongly compressed along the x and y directions and have degrees of freedom only along the z direction. The value of ω_{xy} in (2) is set to 20 au for all calculations and it is not indicated explicitly hereafter. A Gaussian potential has been chosen as the confining potential, that is approximated in the low energy region by a harmonic-oscillator potential typically used for modeling semiconductor quantum dots [25, 15, 4]. The Gaussian potential (2) is characterized by two parameters, namely, by the strength of confinement ω_z and the *anharmonicity* α [21]. Introducing anharmonicity into the confining potential is important for simulating realistic confining potentials [26]. The parameter ω_z is the frequency of the harmonic oscillator obtained by a quadratic approximation to the Gaussian potential and the parameter α is defined by $\alpha = \omega_z/D$ where D is the depth of the Gaussian potential. The total energies and wavefunctions of the Hamiltonian (1) have been calculated as the eigenvalues and eigenvectors of the full CI matrix. The results are presented in atomic units and can be scaled by the effective Bohr radius of 9.79 nm and the effective Hartree energy of 11.9 meV for GaAs semiconductor quantum dots [27, 28].

In order to describe properly the wavefunction of a few electrons confined in a strongly anisotropic, long and narrow space a set of properly chosen Cartesian anisotropic Gaussian-type orbitals (c-aniGTOs) [17] has been adopted as a basis set to expand the one-electron orbital space. Unlike the standard Gaussian-type orbitals the c-aniGTOs can be easily fitted to the anisotropic confining potential by adjusting the three exponents ζ_x, ζ_y and ζ_z independently. A c-aniGTO basis set can be transformed into a set of eigenfunctions of the corresponding three-dimensional anisotropic harmonic oscillator [17]. Therefore, such a basis set is also useful for calculating with high accuracy eigenvalues and eigenfunctions of atoms in strong magnetic fields [29–32] and of semiconductor quantum dots [33, 34].

In the present study a c-aniGTO basis set has been placed at the center of the confining potential, i.e. at the origin of the Cartesian coordinate system. The orbital exponents for the x and y directions have been chosen as $\omega_{xy}/2$ while those for the z direction accounting for the Gaussian potential have been determined in the same way as described in a previous study [24]. Since ω_{xy} is much larger than ω_z, only functions *without* nodes along the x and y directions have been selected and used in the basis sets [18, 24, 21]. The size of the basis set has been determined through an examination of the convergence of the energies calculated by stepwise increasing the size of the basis set. The convergence for three electrons with $(D, \omega_z) = (4.0, 0.1)$ is displayed in figure 1. In this figure the number of basis functions, indicated by the number in the round brackets, was increased stepwise by adding a new function with an additional node to the previous basis set. It is noted that the maximum number of nodes in a function in the basis set, m, is related to the total number of basis functions n by $m = n - 1$. Therefore, in the language of standard quantum chemical basis sets, the largest basis set of 13 functions in figure 1 includes a function with an angular momentum quantum number l as large as 12. As shown in the figure the energy-level structure becomes stabilized as the number of basis functions increases. The maximum deviation of the energy levels covered in figure 1 was shown to be smaller than 3.5×10^{-4} for the results obtained by using basis sets with 13 and 14 functions, respectively. For the rest of the calculations in this study for three electrons the basis set of 14 functions has been used.

3. Results and discussion

3.1. Energy spectrum

The energy spectra of three electrons confined by the quasi-one-dimensional Gaussian potentials with $(D, \omega_z) = (200.0, 5.0)$, $(40.0, 1.0)$ and $(4.0, 0.1)$ have been calculated

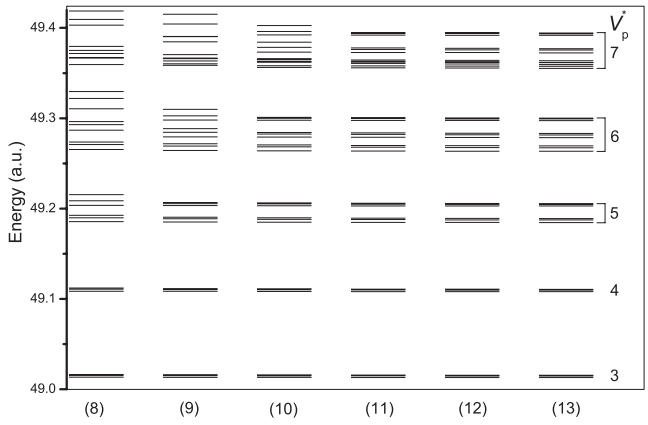

Figure 1. Energy spectrum of the low-lying states of three electrons confined in a quasi-one-dimensional Gaussian potential with $(D, \omega_z, \omega_{xy}) = (4.0, 0.1, 20.0)$ for different-size basis sets. The number in the round brackets specifies the total number of basis functions and the parameter v_p^* specifies the *extended* polyad quantum number (see text).

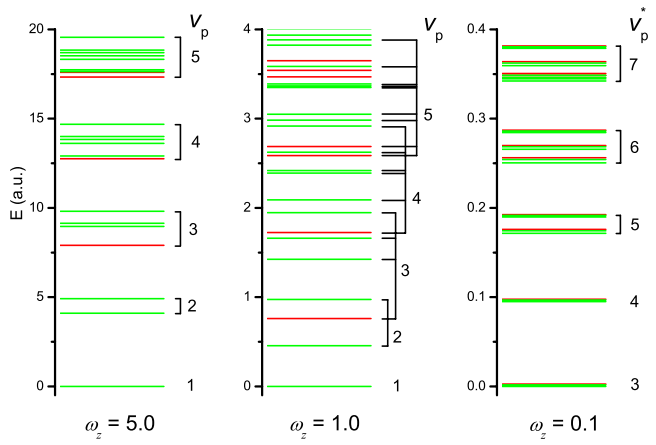

Figure 2. Energy spectrum of three electrons confined by a quasi-one-dimensional Gaussian potential with different strengths of confinement, ω_z, represented as relative energies from the ground state. The anharmonicity parameter α of the Gaussian potential is 0.025 for all cases. The doublet and quartet levels are indicated by green and red lines, respectively, in color or by light and dark lines, respectively, in grayscale. The vertical axis of each of the three energy diagrams is scaled by ω_z so that the energy of the ground state and the excitation energy of four quanta of ω_z are at the same level of the vertical axis, respectively.

and are displayed in figure 2. The anharmonicity parameter α is 0.025 for all cases of (D, ω_z). This corresponds to a relatively harmonic shape of the Gaussian potential. The vertical axis of each of the three energy diagrams is scaled by ω_z, as in our previous study, so that the energy of the ground state and the excitation energy of four quanta of ω_z are at the same level of the vertical axis, respectively [21]. Therefore, *if* there is no electron–electron interaction all three energy spectra will look identical in this representation. The chosen ω_z values of 5.0, 1.0, and 0.1 correspond, respectively, to three regimes of the strength of confinement, namely, large, medium, and small [21]. The classification of the three regimes is defined by the relative importance of the one-electron energy E_1 compared to the two-electron energy E_2. The one-electron energy is scaled by ω_z as $E_1 \sim \omega_z$, since the eigenenergy of the one-dimensional harmonic oscillator is given by $\omega_z(n+\frac{1}{2})$, where n denotes the harmonic-oscillator quantum number. A scaling law for the two-electron energy E_2 may be derived by considering the size of the system as follows [14]: the characteristic length l_z of the system along the z direction is related to ω_z by $l_z \sim 1/\sqrt{\omega_z}$ since the probability distribution of the one-dimensional harmonic-oscillator ground state with the frequency ω_z is proportional to $\exp[-\frac{1}{2}\omega_z z^2]$. On the other hand, since electrons inside the dot would try to keep away from each other, the inter-electron distance may be estimated to be roughly equal to the length of the system l_z. Therefore, the two-electron energy, which is inversely proportional to the length of the system as $E_2 \sim 1/l_z$, is scaled by ω_z as $E_2 \sim \sqrt{\omega_z}$. Thus, the one-electron energy E_1 dominates the two-electron energy E_2 for $w_z \gg 1.0$ (large ω_z), its contribution to the total energy becomes similar to E_2 for $w_z \sim 1.0$ (medium ω_z), and it becomes dominated by E_2 for $w_z \ll 1.0$ (small ω_z).

As shown in figure 2, the energy-level structure changes drastically for different strengths of ω_z, indicating that the effect of electron–electron interaction on the spectrum changes strongly for different ω_z as observed previously for the two-electron case [21]. The energy spectrum for $\omega_z = 5.0$ displayed on the left-hand side of figure 2 shows a band structure in which energy levels having the same *polyad quantum number* v_p indicated by the number on the right-hand side of each band lie close to each other while those with different values of v_p are well separated from each other. The polyad quantum number was introduced in previous studies [24, 21] and specifies in the present model the total number of nodes in the leading configuration of the CI wavefunctions.

In this large confinement regime of $\omega_z = 5.0$, the energy spectrum is dominated by the one-electron confining potential and the electron interaction potential acts only as a perturbation to it, as in the energy spectra of multiply charged atomic ions. Therefore the zeroth-order Hamiltonian for the system can be approximated by a sum of the three harmonic-oscillator Hamiltonians as

$$\mathcal{H}_0 = \sum_{i=1}^{3}\left[-\frac{1}{2}\left(\frac{\partial}{\partial z_i}\right)^2 + \frac{1}{2}\omega_z^2 z_i^2\right], \tag{3}$$

where the x and y degrees of freedom are neglected and the Gaussian potential along the z direction is approximated by a harmonic oscillator with the frequency ω_z. The energy of the Hamiltonian (3) is written in terms of v_p as

$$E_{n_1,n_2,n_3} = \omega_z\left[v_p + \tfrac{3}{2}\right], \tag{4}$$

with

$$v_p = n_1 + n_2 + n_3, \tag{5}$$

where n_1, n_2, and n_3 represent the harmonic-oscillator quantum numbers for electrons 1, 2, and 3, respectively. Therefore, energy levels with the same value of v_p are degenerate. It is noted however that not all possible combinations of (n_1, n_2, n_3) can be realized as quantum states

due to the Pauli principle. For constructing actual electron quantum states for the Hamiltonian (3) it is convenient to use a convention in which spatial orbital configurations are specified using three harmonic-oscillator quantum numbers, either by $|n_1, n_2, n_3\rangle$ where $0 \leqslant n_1 < n_2 < n_3$ or by $|n_1, n_2^2\rangle$ where $0 \leqslant n_1, n_2$ and $n_1 \neq n_2$. The first inequality, $0 \leqslant n_1 < n_2 < n_3$, is imposed in order to remove redundancy in the configurations since permutations of the electron coordinates are performed in the process of antisymmetrization to form configuration state functions. The former configuration is constructed of three different orbitals and can be coupled both to the two types of doublet spin functions and the one type of quartet spin function, while the latter configuration has a doubly occupied orbital and can be coupled only to the one type of doublet spin function, forming a *two-electron singlet* between the electrons residing in the doubly occupied orbital [42]. Therefore the lowest energy configuration $|1, 0^2\rangle$ is a doublet state with the polyad quantum number 1 as shown in figure 2. On the other hand, the lowest quartet state $|0, 1, 2\rangle$ has the polyad number 3 and therefore quartet states first appear in the polyad manifold of $v_\mathrm{p} = 3$. The splitting of levels belonging to the same v_p manifold observed in the energy spectrum of the large confinement regime of $\omega_z = 5.0$ is due to the perturbation by the electron–electron interaction.

As ω_z decreases the splitting of levels within the polyad manifolds becomes larger and energy levels belonging to adjacent polyad manifolds start to overlap with each other as observed in the spectrum for the medium regime of $\omega_z = 1.0$. Nevertheless, the energy spectrum can still be interpreted by using the polyad quantum number v_p since the polyad band structure is still recognizable, as shown in figure 2. Another interesting observation made in this figure is that the quartet levels tend to be located lower than the doublet levels as ω_z becomes smaller. For example, the lowest and second lowest quartet levels located at the bottom of the polyad manifold of $v_\mathrm{p} = 3$ and 4, respectively, for $\omega_z = 5.0$ appear between the doublet levels of $v_\mathrm{p} = 2$ and 3, respectively, for $\omega_z = 1.0$.

As ω_z decreases further, energy levels belonging to different polyad manifolds overlap with each other more strongly and the energy spectrum apparently becomes complicated. On the other hand, the energy spectrum in the small confinement regime of $\omega_z = 0.1$ displayed on the right-hand side of figure 2 has a regular and harmonic band spectrum with a band-gap energy close to ω_z. This observation is similar to the result for the two-electron system in a previous study, in which it was shown that the energy spectrum undergoes a transition to a regular and harmonic band spectrum consisting of singlet–triplet doublets at the small limit of confinement [21]. It is noted that this energy spectrum apparently looks similar to that for $\omega_z = 5.0$ but differs in that all levels form nearly degenerate *triplets*, each of which consists of a pair of doublet states and a quartet state that have belonged to different v_p manifolds for the larger ω_z regimes. A similar triplet structure was reported previously for three electrons confined in a quasi-one-dimensional rectangular potential well [14, 35] as a precursor of the Wigner lattice [20]. Therefore, the observed triplet energy-level structure can be considered as a general trend for weakly confined quasi-one-dimensional three-electron systems. It is also noted that the number of levels belonging to each band as counted from the lowest band is 3, 3, 6, 9, and 12 for $\omega_z = 0.1$ while the corresponding number is 1, 2, 4, 6, and 9, respectively, for $\omega_z = 1.0$ and 5.0.

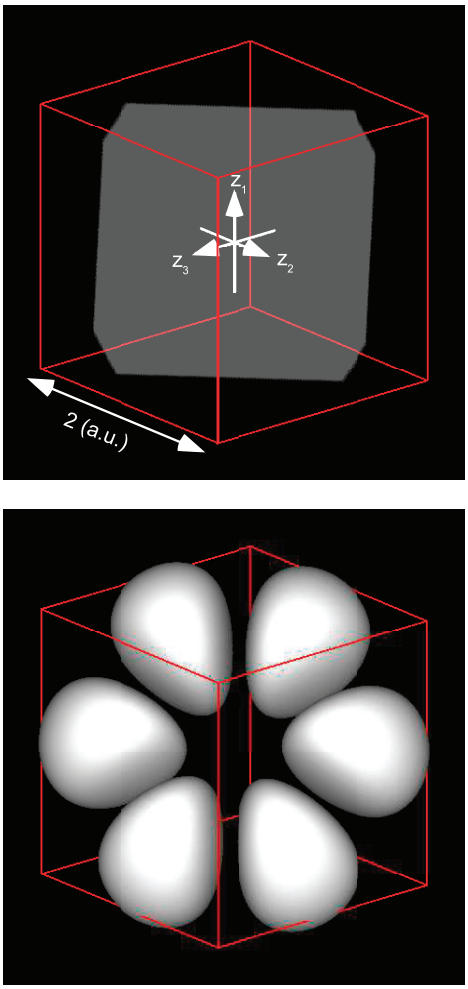

Figure 3. Three-dimensional Cartesian coordinate system for displaying the three-electron wavefunctions (upper figure). The z coordinate of the ith electron is denoted z_i ($i = 1, 2, 3$). The side length of the red cube is 2 au. The gray plane represents the *internal plane* defined by the equation $z_1 + z_2 + z_3 = 0$. It passes through the origin of the coordinate system and is normal to the vector (1, 1, 1). As an example the square-density plot of the three-electron wavefunction for the lowest quartet $^4[0, 3, 0]$ state is displayed (lower figure). The density at the surface is 5.0×10^{-2}.

3.2. Three-electron wavefunctions

In order to understand the origin of the regular band structure with triplets observed in the energy spectrum for $\omega_z = 0.1$ in figure 2, the three-electron wavefunctions have been constructed and displayed in a three-dimensional orthogonal coordinate system described in the upper part of figure 3. The coordinate system in this figure is left handed due to a matter of the graphical software, but the following analysis does not depend on the choices of the coordinate. The wavefunctions are plotted as square density in the three coordinates z_1, z_2 and z_3 by integrating over the remaining six spatial coordinates

of x_i and y_i ($i = 1$, 2 and 3) and over the spin coordinates, respectively. As an example, the square-density plot of the wavefunction of the lowest quartet state for $\omega_z = 5.0$ is displayed in the lower part of figure 3. The wavefunction of this lowest quartet state has three *nodal planes*, which divide the wavefunction into six lobes. The nodal planes of a wavefunction are defined, like *nodal lines* in a previous study, by the planes along which the density of the wavefunction is exactly zero. Since this state has three nodal planes, the polyad quantum number is three, as discussed in the previous section.

In order to make a correspondence between the density distribution of the wavefunction and the underlying correlated motion of the three electrons it is helpful to examine the cross-section of the density distribution by the *internal plane*, which is defined by the equation

$$z_1 + z_2 + z_3 = 0, \tag{6}$$

and is indicated by a gray plane in the upper part of figure 3. This plane cuts all six lobes of the wavefunction of the lowest quartet state in the middle. The meaning of the internal plane for analyzing the correlated motion of three electrons becomes clear by transforming the independent-electron coordinates (z_1, z_2, z_3) into correlated coordinates (z_a, z_b, z_c) by the unitary transformation defined as

$$\begin{aligned} z_a &= \tfrac{1}{\sqrt{3}}[z_1 + z_2 + z_3], \\ z_b &= \tfrac{1}{\sqrt{6}}[2z_1 - z_2 - z_3], \\ z_c &= \tfrac{1}{\sqrt{2}}[z_2 - z_3]. \end{aligned} \tag{7}$$

The z_a coordinate defined by the first line is proportional to the *center-of-mass* coordinate along which the three electrons move in the same direction. The internal plane defined by (6) is normal to z_a. Therefore, this plane is spanned by the remaining two coordinates z_b and z_c. Since the coordinate z_a represents the center-of-mass degree of freedom, the internal plane represents the internal degrees of freedom for the three electrons. The cross-section of the wavefunction of the lowest quartet state with respect to this internal plane is displayed in figure 4. It consists of six parts, as is obvious from inspecting the nodal pattern of the wavefunction displayed in figure 3. The three dotted lines dividing the cross-section into six parts represent the lines of intersection of the three nodal planes with the internal plane. They coincide in the present case with the lines along which the electron–electron interaction potential becomes infinite, namely, $z_1 - z_2 = 0$, $z_1 - z_3 = 0$, and $z_2 - z_3 = 0$, respectively. The two solid lines represent the projection of the z_2 and z_3 axes onto the internal plane. These two lines are obtained from (7) by putting $z_a = 0$ and solving the simultaneous equations for z_2 and z_3 as

$$\begin{aligned} z_2 &= \tfrac{1}{\sqrt{2}}\left[z_c - \tfrac{1}{\sqrt{3}}z_b\right], \\ z_3 &= -\tfrac{1}{\sqrt{2}}\left[z_c + \tfrac{1}{\sqrt{3}}z_b\right]. \end{aligned} \tag{8}$$

Along the z_2 axis the z_3 coordinate is always zero. Therefore, the z_2 line in figure 4 is obtained by putting $z_3 = 0$ in the second line of equations (8), which results in $z_c + \frac{1}{\sqrt{3}}z_b = 0$. Similarly, the z_3 line is obtained by putting $z_2 = 0$ in the first line of equations (8), resulting in $z_c - \frac{1}{\sqrt{3}}z_b = 0$. By using these two lines, that are the projection of the z_2 and z_3 axes onto the internal plane, respectively, each point on the internal plane (z_c, z_b) can be translated into the independent-electron coordinates (z_1, z_2, z_3) by the following procedure. As demonstrated in figure 4, the projection of point A parallel to the two solid lines onto these two lines themselves results in the coordinates A_2 and A_3, respectively. The z_2 and z_3 coordinates of point A are obtained by scaling the resultant coordinates A_2 and A_3 by $\frac{1}{\sqrt{2}}$. From (6) the coordinate of electron 1 is obtained as $z_1 = -(z_2 + z_3)$. In the case of the above example the z_2 coordinate of point A takes a positive value, while the z_3 coordinate takes a negative value with the same magnitude as z_2, resulting in a zero value for the z_1 coordinate. Therefore, the configuration of the three electrons corresponding to point A is that electron 2 resides at a point on the positive z axis, electron 3 at the point on the negative z axis with the same distance from the origin as electron 2, and electron 1 resides at the origin of the z axis.

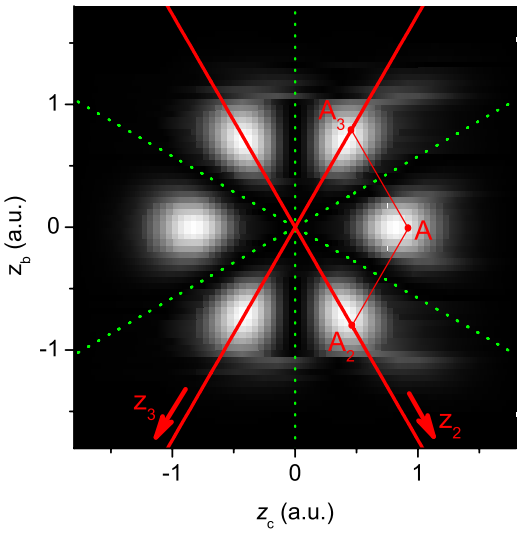

Figure 4. Cross-section with respect to the *internal plane* of the square-density plot of the wavefunction of the lowest quartet $^4[0, 3, 0]$ state displayed in figure 3. The vertical and horizontal axes represent the *internal coordinates* of the electrons defined by $z_b = (2z_1 - z_2 - z_3)/\sqrt{6}$, and $z_c = (z_2 - z_3)/\sqrt{2}$, respectively. The three green dotted lines represent the lines along which the electron–electron interaction potentials become infinity. The two red lines labeled by arrows z_2 and z_3 represent the projection of the z_2 and z_3 axes onto the internal plane.

The assignment of quantum numbers to the wavefunction of the lowest quartet state displayed in figure 3 can be made by inspecting the nodal pattern of the three-dimensional square-density plot of wavefunction and its cross-section with respect to the internal plane as follows. The wavefunction of this state has no nodal plane along the z_a coordinate. Therefore, the quantum number for the *center-of-mass mode*, $n_{\text{c.m.}}$, is zero. On the other hand, the wavefunction has three nodal planes intersecting the internal plane, indicating that three quanta can

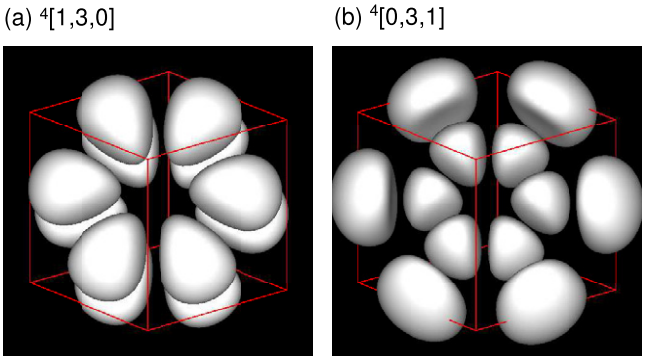

Figure 5. The square-density plot of the three-electron wavefunction for the second lowest quartet state (a) and the third lowest quartet state (b) with their assignments $^4[1, 0, 3]$ and $^4[0, 1, 3]$, respectively. The side length of the red cube and the density at the surface (in au) are 2 and 5.0×10^{-2}, respectively.

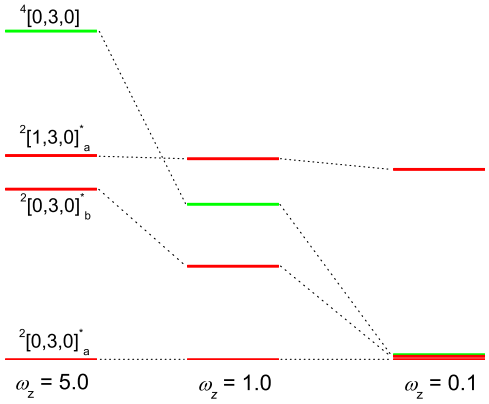

Figure 6. The correspondence of the lowest four energy levels of three electrons confined in a quasi-one-dimensional Gaussian potential with the same anharmonicity α as in figure 2. The red and green levels represent doublet and quartet states, respectively. The vertical axis of each of the energy-level diagrams is scaled by ω_z so that the excitation energy of one quantum of ω_z meets at the same height for different ω_z.

be assigned to some internal degrees of freedom. The cross-section has a sixfold axial symmetry and each center of the six lobes can be obtained by stepwise rotating point A by 60° anticlockwise. By applying an analysis similar to that made for point A to the other five centers, the configuration of the three electrons, (z_1, z_2, z_3), corresponding to each center is obtained as $(0, a, -a)$, $(a, 0, -a)$, $(a, -a, 0)$, $(0, -a, a)$, $(-a, 0, a)$ and $(-a, a, 0)$, where the first is the configuration of point A with $a > 0$. This indicates that the nodal pattern in figure 4 corresponds to a permutational motion of three electrons. Therefore, the wavefunction of the lowest quartet state has three quanta in the *permutation mode* n_p. Since the internal plane is two dimensional, there should be another mode that is not excited in the lowest quartet state. The square-density plot of the wavefunctions for the second and third lowest quartet states is displayed in figures 5(a) and (b), respectively. The nodal pattern of the wavefunction for the second lowest quartet state, figure 5(a), shows an extra nodal plane other than the three nodal planes of the lowest quartet state. This nodal plane is perpendicular to the z_a coordinate. Therefore, it represents a quantum state that is obtained from the lowest quartet state by exciting one quantum into the center-of-mass mode. On the other hand, the nodal pattern of the third lowest quartet state, figure 5(b), shows a new nodal plane which intersects the internal plane circularly. Since this nodal plane represents a radial excitation within the internal plane, the electron mode corresponding to this nodal plane represents a *breathing* motion of the three electrons in which the inter-electron distances change by keeping their relative ratios fixed. Therefore, this new internal mode may be termed as the *breathing mode* and its quantum number will be denoted by n_b. These three-electron modes, the center-of-mass, permutation, and breathing modes, can be regarded as the *normal modes* of the quartet states of three electrons, since the quantum states can be specified uniquely by counting the number of nodal planes independently for the three modes. Therefore, the three-electron quartet wavefunctions will be assigned hereafter by the notation $^{2S+1}[n_\mathrm{c.m.}, n_\mathrm{p}, n_\mathrm{b}]$ where $2S + 1$ denotes the spin multiplicity. By using this notation the lowest, second lowest and third lowest quartet states are assigned as $^4[0, 3, 0]$, $^4[1, 3, 0]$ and $^4[0, 3, 1]$, respectively. It is noted that the polyad quantum number v_p is calculated from these three quantum numbers, $n_\mathrm{c.m.}$, n_p and n_b, by

$$v_\mathrm{p} = n_\mathrm{c.m.} + n_\mathrm{p} + 2n_\mathrm{b}. \tag{9}$$

The quantum number for the breathing mode contributes to the sum twice as many as that for the center-of-mass mode and the permutation mode, since the nodal plane of the breathing mode cuts the two-dimensional internal plane circularly like the breathing mode for the Hartree–Fock orbitals in quasi-two-dimensional circular quantum dots [24].

3.3. Interpretation of spectra

The correspondence of the lowest four energy levels of three electrons for different ω_z is displayed in figure 6. The assignment in this figure for the lowest quartet state is the same as defined in the previous section, while those for the three doublet states have been made by inspecting the nodal pattern of their wavefunctions at $\omega_z = 0.1$. The vertical energy axis is scaled in the same way as in figure 2 so that the excitation energy of one quantum of ω_z is at the same level for different ω_z. It can be seen from figure 6 that the lowest two doublet states, $^2[0, 3, 0]^*_a$ and $^2[0, 3, 0]^*_\mathrm{b}$, and the lowest quartet state $^4[0, 3, 0]$ get closer as ω_z decreases and finally become degenerate at $\omega_z = 0.1$. On the other hand, the position of the third lowest doublet state $^2[1, 3, 0]^*_a$ is relatively insensitive to a variation of ω_z, indicating that the excitation energy from the lowest doublet state scaled by ω_z is not affected strongly by the variation of ω_z.

In order to understand these observations, i.e. the degeneracy among the two doublet and one quartet states for small ω_z and the insensitivity of the position of the third lowest doublet state with respect to the change of ω_z, the wavefunctions of the lowest four states for different ω_z have been constructed and displayed in figure 7. In this figure the

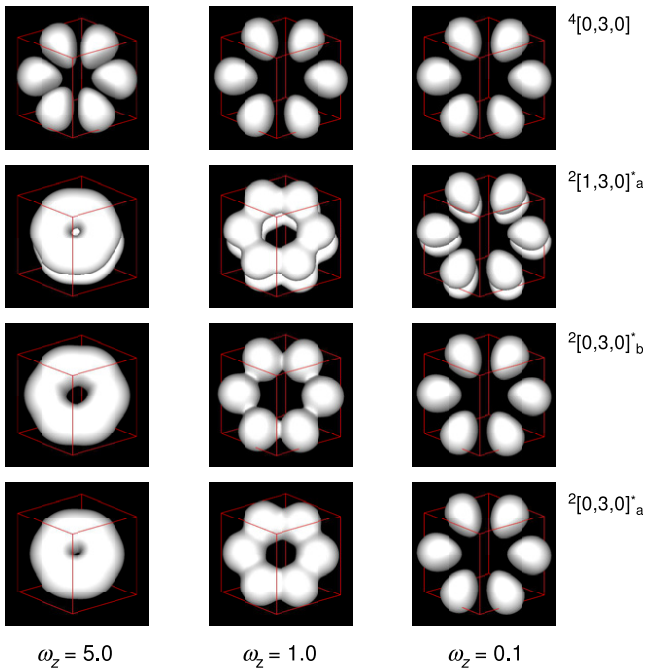

Figure 7. The square-density plot of the three-electron wavefunctions for the lowest four states displayed in figure 6 for different strengths of confinement ω_z. The density at the surface and the side length of the cube (in au) are $(5.0\times10^{-2}, 2.0)$, $(1.0\times10^{-2}, 4.0)$ and $(1.0\times10^{-4}, 16.0)$ for $\omega_z = 5.0$, 1.0 and 0.1, respectively.

wavefunctions are plotted in a similar way as in figure 3 but the density ρ at the surface of each wavefunction and the side length d of the cube differ for different ω_z so that the nodal patterns in the wavefunctions can be clearly identified. The chosen values are $(\rho, d) = (5.0\times10^{-2}, 2.0)$, $(1.0\times10^{-2}, 4.0)$ and $(1.0\times10^{-4}, 16.0)$ for $\omega_z = 5.0$, 1.0 and 0.1, respectively.

The wavefunction of the lowest quartet state for $\omega_z = 5.0$, displayed uppermost in the left side column of figure 7, has three nodal planes as explained in the previous section. In general, the spatial part and the spin part of wavefunctions for quartet states of three electrons are separated from each other and the spin part of the wavefunctions is totally symmetric with respect to interchanging any two spin coordinates. Therefore, the spatial part of quartet wavefunctions should be antisymmetric with respect to an interchange of any two-electron coordinates because of the Pauli exclusion principle. It is noted that the transposition within two-electron coordinates, (z_1, z_2), (z_1, z_3), and (z_2, z_3), in a spatial wavefunction can be performed by reflecting the wavefunction with respect to the plane along which the electron–electron interaction potentials become infinite, namely $z_1 - z_2 = 0$, $z_1 - z_3 = 0$, and $z_2 - z_3 = 0$, respectively. Therefore, the quartet wavefunction has to always have these three planes as nodal planes, since it has to change signs with respect to a reflection about any of these three planes. In a traditional terminology these three nodal planes may be termed as Fermi holes or exchange holes of indistinguishable Fermi particles.

On the other hand, in the case of doublet states of three electrons the spatial and spin parts of the wavefunctions are mixed and not separable in general. Therefore, unlike quartet wavefunctions, the doublet wavefunctions displayed in figure 7 for $\omega_z = 5.0$ do not have the three nodal planes of Fermi holes, since the spatial part of the wavefunctions does not change its signs with respect to a reflection about any of these three planes. Because of this nonseparability it is difficult to assign quantum numbers to the doublet wavefunctions from their nodal pattern in the spatial distribution. The assignments of quantum numbers to the three lowest doublet wavefunctions in figure 7, $^2[0, 3, 0]^*_a$, $^2[0, 3, 0]^*_b$, and $^2[1, 3, 0]^*_a$, respectively, have been therefore made by inspecting the nodal pattern of the wavefunctions for the small limit of confinement $\omega_z = 0.1$, at which the wavefunctions of the doublet states have a clear nodal pattern for the reason which will be given below. Instead of having a clear nodal pattern the wavefunction of the lowest doublet state at $\omega_z = 5.0$ has a sharp decrease of density at the center, as displayed at the bottom of the left-hand column of figure 7. The wavefunction of the second lowest doublet state at $\omega_z = 5.0$ also has a sharp decrease of density at the center with a larger magnitude. These sharp decreases of density for the lowest and second lowest doublet states are explained by the following considerations: the lowest and the second lowest doublet states have the leading configurations $|1, 0^2\rangle$ and $|0, 1^2\rangle$, respectively. The lowest one-electron orbital bound in a one-dimensional harmonic-oscillator potential has no node while the second lowest orbital has one node at the center. Since both of the configurations, $|1, 0^2\rangle$ and $|0, 1^2\rangle$, have one and two electrons that have a node at the origin of the z axis, respectively, the density distribution of their wavefunctions about the origin should be very small, with a magnitude for $|0, 1^2\rangle$ smaller than for $|1, 0^2\rangle$. Therefore, the sharp decrease of density observed at the center of these two lowest doublet wavefunctions can be interpreted as a remnant of the node of the second lowest one-electron orbital.

The nodal pattern of the wavefunction of the third lowest doublet state at $\omega_z = 5.0$ has one significant difference compared to the other doublet wavefunctions in that it has a nodal plane along a line perpendicular to the internal plane, namely, the z_a axis. Aside from this node the wavefunction of the third doublet state has a similar nodal pattern as the lowest doublet state. Therefore, the third doublet state is obtained from the lowest doublet state by exciting one quantum into the center-of-mass mode n_a. According to the generalized Kohn theorem [36–38, 25, 39–41], if the confining potential is purely harmonic, the energy for a center-of-mass excitation is exactly equal to the strength of the confinement, irrespective of the number of electrons and the form of electron–electron interaction. In the present case the Gaussian confining potential is approximated well for the low energy region by a harmonic-oscillator potential with ω_z. Therefore, the excitation energy from the lowest doublet state to the third doublet state is roughly equal to ω_z for all regimes of ω_z. This explains the relative insensitivity of the position of the third doublet state with respect to the change of ω_z as observed in figure 6.

Another interesting observation made in the wavefunctions of figure 7 is that the wavefunctions of the two lowest doublet states for $\omega_z = 0.1$ have almost identical spatial distributions in spite of having significant differences for larger ω_z.

Table 1. Zeroth-order energy levels for the large ω_z regime.

v_p	N_p [a]	$\|n_1, n_2^2\rangle$	$\|n_1, n_2, n_3\rangle$
1	1	$\|1, 0^2\rangle$	
2	2	$\|2, 0^2\rangle$	
		$\|0, 1^2\rangle$	
3	4	$\|3, 0^2\rangle$	$\|0, 1, 2\rangle$
4	6	$\|4, 0^2\rangle$	$\|0, 1, 3\rangle$
		$\|2, 1^2\rangle$	
		$\|0, 2^2\rangle$	
5	9	$\|5, 0^2\rangle$	$\|0, 1, 4\rangle$
		$\|3, 1^2\rangle$	$\|0, 2, 3\rangle$
		$\|1, 2^2\rangle$	

[a] Number of levels belonging to each v_p manifold.

By following the evolution of the two lowest doublet wavefunctions from $\omega_z = 5.0$ to 0.1, it can be seen that the density of the wavefunctions tends to decrease along the three nodal planes of the Fermi holes, namely $z_1 - z_2 = 0$, $z_1 - z_3 = 0$ and $z_2 - z_3 = 0$, as ω_z decreases, and that at $\omega_z = 0.1$ the three planes become apparently the nodal planes of the doublet wavefunctions, although the sign of the wavefunctions should not change with respect to a reflection about these three planes. In order to understand the origin of the decrease of density in the doublet wavefunctions along these three nodal planes, the cross-section of the sum of the one- and two-electron potential functions in the Hamiltonian (1) with respect to the internal plane,

$$V(z_b, z_c) = \frac{1}{2}\omega_z^2[z_b^2 + z_c^2] + \frac{2}{|\sqrt{6}z_b + \sqrt{2}z_c|} + \frac{2}{|\sqrt{6}z_b - \sqrt{2}z_c|} + \frac{1}{|\sqrt{2}z_c|}, \quad (10)$$

where the Gaussian potential is approximated by a harmonic-oscillator potential with ω_z, has been calculated and displayed in figure 8 for $\omega_z = 5.0$, 1.0 and 0.1, respectively. In all three cases displayed in figure 8 the maximum potential height is $20 \times \omega_z$ and the domain of the coordinates z_b and z_c is chosen such that for the one-dimensional harmonic-oscillator potential the classical turning points for an energy of $20 \times \omega_z$ coincide with the limits of the domain. In this representation the energy contours for the one-electron part of the potential, i.e. the first term on the right-hand side of (10), are identical for different values of ω_z. Therefore, differences in the contours among different ω_z must be ascribed to the electron–electron interaction potentials. It is noted that the three lines separating the contours into six regions are the *potential walls* of the electron–electron interaction potentials along which the second to fourth terms on the right-hand side of (10) become infinite. As shown in figures 8(a)–(c) these potential walls become thicker as ω_z decreases from 5.0 to 0.1. This indicates that the wavefunctions bound in this potential are influenced by the electron–electron interaction potentials more strongly for smaller ω_z.

In the large ω_z regime of figure 8(a) the potential walls of the electron–electron interaction are so thin that electrons can tunnel through them easily. Therefore, the corresponding

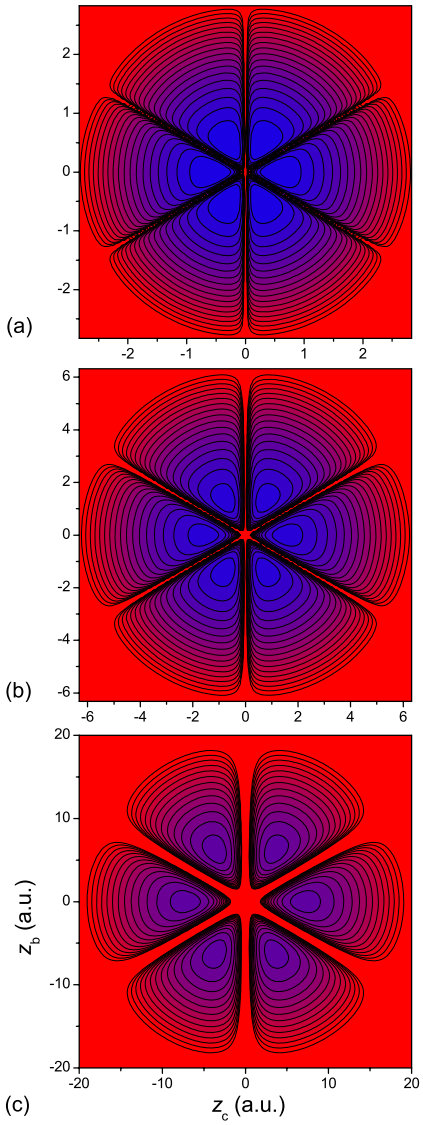

Figure 8. The two-dimensional contour plot of the sum of the harmonic oscillator and of the electron repulsion potentials with respect to the *internal plane* for $\omega_z = 5.0$ (a), 1.0 (b), and 0.1 (c). The maximum potential height displayed is $\omega_z \times 20$ for all cases. The three lines separating the contours into six regions represent the potential walls of the electron repulsion potentials.

wavefunctions are influenced little by the potential walls, as displayed in figure 7. The tunneling manifests itself as splitting of the degenerate zeroth-order levels of each v_p manifold of (4) as displayed in figure 2 for the energy spectrum of $\omega_z = 5.0$. The degeneracy pattern for each v_p manifold can be obtained by counting the number of possible orbital configurations as summarized in table 1. For the lowest two v_p manifolds of $v_p = 1$ and 2, respectively, only the configuration of the type $|n_1, n_2^2\rangle$ is allowed. This configuration can be coupled only to the doublet spin function that forms a two-electron singlet for the pair of electrons 2 and 3 occupying orbital n_2, as mentioned earlier. An explicit form of the spin function can be written by assuming that the magnetic quantum number M of the spin function takes the highest value, i.e. $\frac{1}{2}$ for the doublet state and $\frac{3}{2}$ for the quartet state, respectively. This

assumption does not lose generality since the eigenstates of the present spin-free Hamiltonian (1) should be independent of the orientation of the total spin vector. With this assumption the explicit form of the spin function for quartet states is written as $|\alpha\alpha\alpha\rangle$. In the case of doublet states, on the other hand, there are two linearly independent spin functions for the spin state of $|S, M\rangle = |\frac{1}{2}, \frac{1}{2}\rangle$, namely, $\frac{1}{\sqrt{2}}\alpha(1)(\alpha(2)\beta(3) - \beta(2)\alpha(3))$ and $\frac{1}{\sqrt{6}}(2\beta(1)\alpha(2)\alpha(3) - \alpha(1)\alpha(2)\beta(3) - \alpha(1)\beta(2)\alpha(3))$, respectively [43]. The former spin function (denoted hereafter as $|a\rangle$ for brevity) is a product of the singlet spin function for the electron pair (2, 3) and the α spin function for electron 1, and forms the two-electron singlet for the electron pair 2 and 3 denoted above. Therefore, the orbital configuration of the type $|n_1, n_2^2\rangle$ can be coupled to the $|a\rangle$ spin function, since this function simply changes its signs with respect to an interchange of electron coordinates 2 and 3. On the other hand, it cannot be coupled to the latter spin function (denoted hereafter by $|b\rangle$), since $|b\rangle$ does not change its sign but behaves in a more complicated way with respect to the transposition of electron coordinates 2 and 3. Therefore, the total number of levels for the first and second manifolds in table 1 is calculated to be $N_\mathrm{p} = 1$ and 2, respectively. In the case of the third manifold the two configurations $|3, 0^2\rangle$ and $|0, 1, 2\rangle$ are allowed. From the first configuration of $|3, 0^2\rangle$ only one level can be derived, as in the case of the configurations $|1, 0^2\rangle$ and $|0, 1^2\rangle$. On the other hand, the second configuration $|0, 1, 2\rangle$ can be coupled both to the two doublet spin functions $|a\rangle$ and $|b\rangle$ and to the one quartet spin function $|\alpha\alpha\alpha\rangle$, resulting in a total of three levels. Therefore, the total number of levels for the third manifold is determined to be $N_\mathrm{p} = 4$, as shown in table 1. Similarly, the total number of levels for the fourth and fifth manifolds is calculated to be $N_\mathrm{p} = 6$ and 9, respectively, all of which are consistent with the number of levels indicated in the energy spectrum of figure 2 for $\omega_z = 5.0$.

As ω_z decreases, the potential walls become thicker, as displayed in figure 8(b). Therefore, the doublet wavefunctions tend to have lower density along these potential walls, as shown in figure 7, in order to lower their energy. On the other hand, the quartet wavefunction is affected little by the potential walls, since its density along the potential walls is exactly zero because of the exclusion principle. Therefore, the energy level of the quartet state is more stable than those of the doublet states with respect to the decrease of ω_z. This results in a decrease of the energy difference between the quartet and doublet levels, as shown in figure 6.

In the small confinement regime of $\omega_z = 0.1$ the potential walls become so thick that they can no longer be treated as a perturbation to the confining potential, but become barriers through which electrons can hardly tunnel. Consequently, the wavefunctions of the doublet states have almost no density along the potential walls, as observed in figure 7, and little difference can be seen between the wavefunctions of the lowest two doublet states and the lowest quartet $^4[0, 3, 0]$ state except for their phases. By using the similarity of density distributions to the quartet wavefunction the wavefunctions of the lowest and the second lowest doublet states can be assigned as $^2[0, 3, 0]^*_a$ and $^2[0, 3, 0]^*_b$, respectively, where a and b denote abbreviations for distinguishing different doublet spin states and $*$ denotes that it is an *extended* assignment. The reason for the three states $^2[0, 3, 0]^*_a$, $^2[0, 3, 0]^*_b$ and $^4[0, 3, 0]$ having almost the same energy regardless of their phase differences can be rationalized as follows: the nodal pattern of the wavefunction of the lowest quartet $^4[0, 3, 0]$ state can be interpreted as a spatial configuration of three electrons in which one electron resides at the origin of the z axis while the other two electrons reside at either the positive or the negative z axis, respectively, as discussed in section 3.2. In the weak confinement regime of $\omega_z = 0.1$ the mean inter-electron distance is very large. Therefore, the energy of the three electrons depends little on the mutual orientation of their electron spins. A similar argument can be applied to more than three electron cases. In the case of four electrons the number of electron–electron interaction potentials is six, which is calculated as the number of combinations choosing two electrons out of four different electrons. This number is equal to the sum of the numbers of linearly independent spin functions of four electrons, namely, two spin functions for singlet states, three for triplet, and one for quintet. At the limit of small confinement ω_z all these spin states of four electrons become degenerate. Therefore the lowest energy level of four electrons is sixfold degenerate, with $v^*_\mathrm{p} = 6$ [44].

Finally, the origin of the harmonic band structure of the energy spectrum with regular intervals of ω_z in the small ω_z regime can also be rationalized by making use of the contour map of the potential function $V(z_\mathrm{b}, z_c)$ displayed in figure 8. The Hamiltonian (1) can be written by using the correlated electron coordinates defined by equations (7) within the one-dimensional harmonic approximation of the confining potential as

$$\mathcal{H}^{\mathrm{harm}}_{1\mathrm{D}} = -\frac{1}{2}\left[\frac{\partial^2}{\partial z_a^2} + \frac{\partial^2}{\partial z_\mathrm{b}^2} + \frac{\partial^2}{\partial z_c^2}\right] + \frac{1}{2}\omega_z^2\left[z_a^2 + z_\mathrm{b}^2 + z_c^2\right] + \frac{2}{|\sqrt{6}z_\mathrm{b} + \sqrt{2}z_c|} + \frac{2}{|\sqrt{6}z_\mathrm{b} - \sqrt{2}z_c|} + \frac{1}{|\sqrt{2}z_c|}. \quad (11)$$

In this Hamiltonian the z_a coordinate, which is proportional to the center-of-mass coordinate of the three electrons, is decoupled from the other degrees of freedom since it does not appear in the electron–electron interaction potentials. Therefore, the center-of-mass mode generates simply the harmonic energy spectrum of ω_z as known from the generalized Kohn theorem. By omitting in equation (11) the z_a dependent terms, it becomes the Hamiltonian of the two-dimensional isotropic harmonic oscillator with modified electron–electron interaction potentials. The corresponding potential is identical to $V(z_\mathrm{b}, z_c)$ displayed in figure 8. In the small confinement regime of figure 8(c) the wavefunctions of electrons bound in this potential have almost no density along the three walls of the electron–electron interaction potentials. It is noted that wavefunctions satisfying this boundary condition are eigenfunctions of the two-dimensional isotropic harmonic oscillator with the angular momentum $|l| = 3$. This constraint on the angular momentum guarantees that the wavefunctions have three nodal lines with an equiangular interval of 120°. The simultaneous eigenstates of the two-dimensional isotropic harmonic-oscillator Hamiltonian,

$$\mathcal{H}^{\mathrm{harm}}_{\mathrm{int},0} = -\frac{1}{2}\left[\frac{\partial^2}{\partial z_\mathrm{b}^2} + \frac{\partial^2}{\partial z_c^2}\right] + \frac{1}{2}\omega_z^2\left[z_\mathrm{b}^2 + z_c^2\right], \quad (12)$$

and of the angular momentum operator,

$$\hat{l} = \frac{1}{\mathrm{i}}\left[z_c\frac{\partial}{\partial z_\mathrm{b}} - z_\mathrm{b}\frac{\partial}{\partial z_c}\right], \tag{13}$$

can be obtained by using the *circular boson* operators [45], defined in the present case by

$$\begin{aligned}\hat{a}_\pm &= \frac{1}{\sqrt{2}}[\hat{a}_c \mp \mathrm{i}\hat{a}_b],\\ \hat{a}_\pm^\dagger &= \frac{1}{\sqrt{2}}[\hat{a}_c^\dagger \pm \mathrm{i}\hat{a}_b^\dagger],\end{aligned} \tag{14}$$

where $\hat{a}_\mathrm{b}$, $\hat{a}_c$ and their Hermitian conjugates are the standard harmonic-oscillator ladder operators defined by

$$\hat{a}_k = \frac{1}{\sqrt{2}}\left[\sqrt{\omega_z}z_k + \frac{1}{\sqrt{\omega_z}}\frac{\partial}{\partial z_k}\right], \tag{15}$$

etc, for $k = b$ and c. It can be shown that the circular boson ladder operators of equations (14) satisfy the usual commutation relation of the harmonic-oscillator ladder operators such as $[\hat{a}_\pm, \hat{a}_\pm^\dagger] = 1$. By using these circular boson operators the two-dimensional harmonic-oscillator Hamiltonian (12) and the angular momentum operator (13) are rewritten as

$$\mathcal{H}_{\mathrm{int},0}^{\mathrm{harm}} = \omega_z[\hat{a}_+^\dagger\hat{a}_+ + \hat{a}_-^\dagger\hat{a}_- + 1], \tag{16}$$

and

$$\hat{l} = \hat{a}_+^\dagger\hat{a}_+ - \hat{a}_-^\dagger\hat{a}_-, \tag{17}$$

respectively. Therefore, the simultaneous eigenstates of the operators (16) and (17) are the direct product of the circular boson number states, $|n_+\rangle|n_-\rangle$. The eigenvalues of the operators are calculated explicitly as

$$E_{\mathrm{int},0}^{\mathrm{harm}} = \omega_z[n_+ + n_- + 1], \tag{18}$$

and

$$l = n_+ - n_-, \tag{19}$$

respectively, where n_+ and n_- are the eigenvalues of the number operator for the $+$ and $-$ bosons, respectively. By choosing $|l| = 3k$ ($k = 1, 2, \ldots$), the eigenenergy of the Hamiltonian (11) in the small ω_z regime is approximated by the following closed form:

$$E_{\mathrm{1D,small}}^{\mathrm{harm}} = \omega_z\left[n_a + 2n + 3k + \tfrac{3}{2}\right], \tag{20}$$

where $n = 0, 1, 2, \ldots$ and n_a denotes the harmonic-oscillator quantum number for the center-of-mass mode. It is noted that the three quantum numbers n_a, n, and k are related to the three normal-mode quantum numbers defined in the previous section by $n_\mathrm{c.m.} = n_a$, $n_\mathrm{b} = n$, and $n_\mathrm{p} = 3k$, respectively. The result (20) shows that energy levels having the same value of $v_\mathrm{p}^* = n_a + 2n + 3k$ have the same energy and that the energy levels form an equispaced band structure with an energy gap of ω_z. The new quantity v_p^* is the *extended* polyad quantum number, which is obtained by counting the total number of nodal planes in the wavefunction, including the three planes of the potential walls for doublet wavefunctions.

Table 2. Possible combinations of quantum numbers (n_a, n, k) in the energy formula (20) for the small ω_z regime.

v_p^*	$N_\mathrm{p}^{*\,\mathrm{a}}$	n_a	n	k
3	3	0	0	1
4	3	1	0	1
5	6	0	1	1
		2	0	1
6	9	0	0	2
		1	1	1
		3	0	1
7	12	1	0	2
		0	2	1
		2	1	1
		4	0	1

[a] Number of levels belonging to each v_p^* manifold.

The degeneracy pattern of the v_p^* manifolds, i.e. 3, 3, 6, 9, and 12, indicated in the energy spectrum of figure 2 for $\omega_z = 0.1$, is obtained by counting the possible combinations of the three quantum numbers (n_a, n, k) for a given value of v_p^* as summarized in table 2. For the lowest two manifolds of $v_\mathrm{p}^* = 3$ and 4 only the two combinations (0, 0, 1) and (1, 0, 1) are possible. Since each combination can be coupled to all three spin functions, i.e. two doublets and one quartet, the resulting number of states is three for both $v_\mathrm{p}^* = 3$ and 4. For the higher manifolds of $v_\mathrm{p}^* = 5$, 6, and 7 the number of possible combinations is two, three, and four, respectively. Therefore, the total number of states belonging to these manifolds is 6, 9, and 12, respectively. All these numbers agree with the number of states indicated in the energy spectrum of figure 2 for $\omega_z = 0.1$.

3.4. Anharmonic case

The energy spectra of three electrons confined by the quasi-one-dimensional Gaussian potentials with $(D, \omega_z) = (50.0, 5.0)$, (10.0, 1.0) and (1.0, 0.1) have been calculated and are displayed in figure 9 in the same way as in figure 2. The anharmonicity parameter is $\alpha = 0.1$ for all cases of (D, ω_z), which corresponds to a relatively anharmonic shape of the Gaussian potential. The value for the anharmonicity parameter has been chosen such that all energy levels displayed in figure 9 are lying below the first ionization limit [24]. When the anharmonicity parameter α becomes larger than this value, some energy levels close to the upper limit of the energy range become unbound. The energy spectra for $\omega_z = 5.0$ and 1.0 displayed in figure 9 show a band structure very similar to that of the corresponding spectra displayed in figure 2. They are characterized by the polyad quantum number v_p, as denoted in the figure. The energy differences between adjacent polyad manifolds are slightly smaller for the spectra shown in figure 9 than for those displayed in figure 2, which is due to the larger anharmonicity of the Gaussian potential for the spectra shown in figure 9. In the case of $\omega_z = 0.1$, a large difference can be observed between the spectra shown in figures 2 and 9 in the higher energy region above $E = 0.3$. In

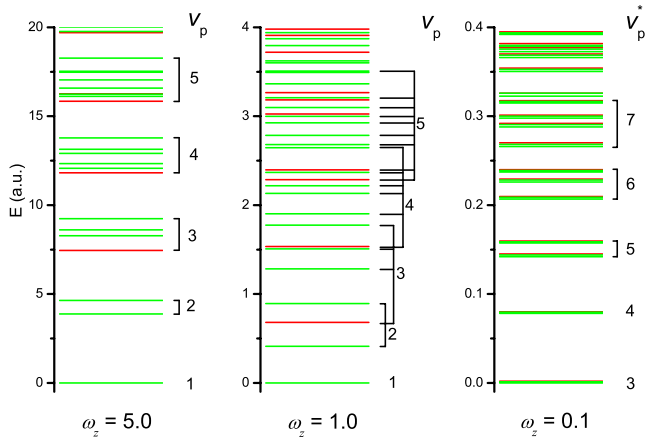

Figure 9. Energy spectrum of three electrons confined by a quasi-one-dimensional Gaussian potential with different strengths of confinement ω. The anharmonicity parameter α of the Gaussian potential is 0.1 for all cases. See the caption of figure 2 for other remarks.

the energy spectrum displayed in figure 2, the polyad manifold of $v_p^* = 7$ is energetically well separated both from the lower- and the higher-lying manifolds, while in the spectrum shown in figure 9 it lies energetically close to the higher-lying manifold. Therefore, effects of coupling between energy levels of different v_p^* manifolds may appear in the electronic wavefunctions.

In order to understand the effect of anharmonicity on the wavefunctions, the square density of the wavefunctions for the four quartet states in the polyad manifold of $v_p^* = 7$, namely, $^4[2, 3, 1]$, $^4[0, 3, 2]$, $^4[1, 6, 0]$, and $^4[0, 6, 0]$, respectively, is displayed in figure 10 for $\alpha = 0.0$ (harmonic) and 0.1 (anharmonic). Unlike the wavefunctions displayed in figure 7, the sign of the wavefunctions, positive or negative, is indicated in figure 10 by red and blue surfaces, respectively. The phase information can be graphically displayed, since the orbital and spin parts of the quartet wavefunctions are separated from each other. As shown in this figure, the assignment of quantum numbers to the wavefunctions can be made uniquely for the harmonic case by counting the number of nodal planes for the three normal modes, i.e. the center-of-mass, permutation and breathing modes. On the other hand, in the case of the wavefunctions for the anharmonic case the nodal planes dividing the wavefunctions are neither simple planes as for the center-of-mass and permutation modes nor cylindrical surfaces as for the breathing mode, but are distorted significantly. The effect of deformation of the nodal planes seems to be larger for the states having excitation into the center-of-mass mode than for the other states. For example, the nodal pattern of the wavefunction of the $^4[0, 3, 2]$ state, which has no excitation into the center-of-mass mode, lie in the internal plane both for the harmonic and anharmonic cases. On the other hand, in the case of the states having excitation into the center-of-mass mode, such as $^4[4, 3, 0]$ and $^4[2, 3, 1]$, it is difficult to count the number of nodal planes along the center-of-mass coordinate for the anharmonic case since it is hard to judge how the nodal planes divide the wavefunction along which coordinate. These

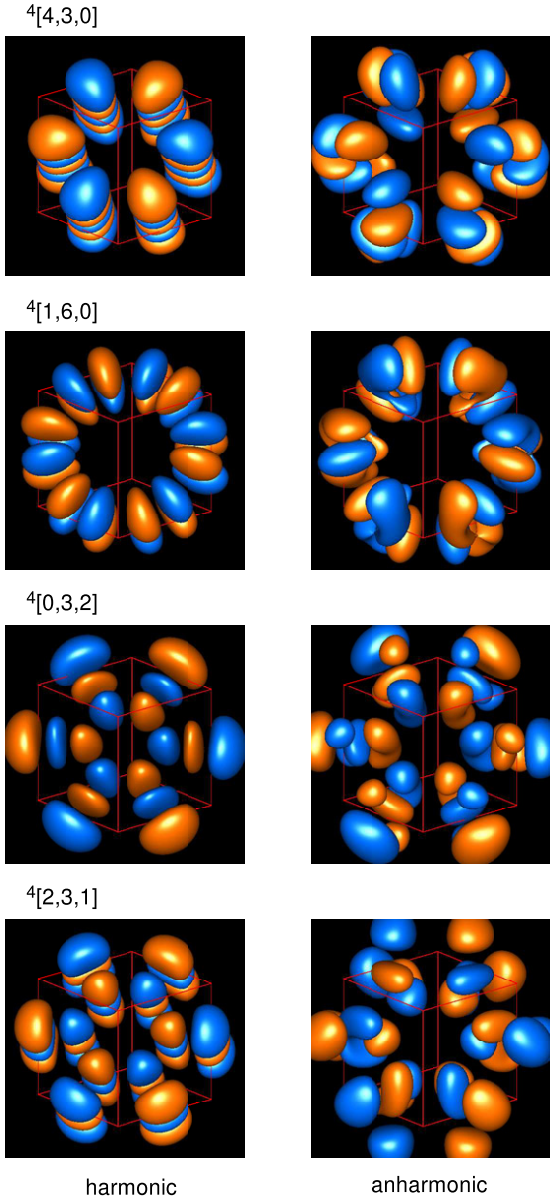

Figure 10. The square-density plot of the three-electron wavefunctions for the four quartet states in the polyad manifold of $v_p^* = 7$, $^4[2, 3, 1]$, $^4[0, 3, 2]$, $^4[1, 6, 0]$, and $^4[0, 6, 0]$, respectively, for $\alpha = 0.0$ (harmonic) and 0.1 (anharmonic). The strength of confinement ω_z is 0.1 for all cases. The density at the surface and the side length of the cube (in au) are 1.0×10^{-4} and 16, respectively. The red and blue surfaces represent the positive and negative phases of the wavefunctions, respectively.

observations indicate that the center-of-mass mode is no longer separable from the internal modes and suggests that a transition from the three normal modes to some new modes occurs as a result of the large anharmonicity in the confining potential, as observed in a previous study for two electrons confined in a quasi-one-dimensional nanostructure [21].

4. Summary

In order to understand general trends of energy spectra of quasi-one-dimensional multi-electron quantum dots, the

energy spectra and wavefunctions of three electrons confined by a quasi-one-dimensional Gaussian potential have been calculated for different strengths of confinement and anharmonicity by using the quantum chemical full configuration interaction method employing reduced Cartesian anisotropic Gaussian basis sets. The most important results of the present study are summarized as follows.

The energy spectra for a nearly harmonic Gaussian potential have been calculated and analyzed for three regimes of confinement strength ω_z, namely, strong ($\omega_z = 5.0$), medium ($\omega_z = 1.0$) and weak ($\omega_z = 0.1$). For the strong confinement the energy spectrum shows a regular band structure with a band-gap close to ω_z. The energy levels of each band are well localized and are characterized by the *polyad quantum number* v_p, defined as the number of the nodal planes dividing the wavefunctions. For the medium confinement the energy spectrum also shows a band structure characterized by v_p, but the splitting of the energy levels belonging to the same v_p manifold is so large that adjacent polyad manifolds get close to each other or even overlap. For the small confinement strength two doublet states and one quartet state which belong to different v_p manifolds of the larger ω_z regimes become nearly degenerate and form a triply degenerate energy level. The energy spectrum in this small confinement regime recovers a band structure with a band-gap energy of about ω_z, as observed for the large confinement regime, but each band is characterized by the *extended* polyad quantum number v_p^*.

The square density of the wavefunctions has been plotted in the three-dimensional (z_1, z_2, z_3) space and its nodal pattern has been examined. From the analysis of the cross-section of the wavefunctions with respect to the internal plane it has been shown that the wavefunctions of quartet states can be assigned uniquely by counting the number of nodal planes for the three normal modes, namely, the center-of-mass, the permutation and the breathing modes. All quartet wavefunctions have three nodal planes originating from exchange holes defined by the equations $z_1 - z_2 = 0$, $z_2 - z_3 = 0$ and $z_3 - z_1 = 0$ along which the electron–electron interaction potentials become infinite. In case of the wavefunctions of doublet states, on the other hand, assignment of quantum numbers based on their nodal pattern is not straightforward, except for the center-of-mass mode, since the spatial part and the spin part of the wavefunctions are mixed and not separable. The density of the doublet wavefunctions along the three nodal planes of the quartet wavefunctions becomes smaller as ω_z decreases and it becomes negligibly small for $\omega_z = 0.1$. The doublet wavefunctions at $\omega_z = 0.1$ have the same number of nodal lines as their counterpart quartet wavefunction of the degenerate triplet using the extended assignment. Their nodal patterns become almost identical to each other except for their phases. The sum of the one- and two-electron potentials projected onto the internal plane shows that the decreasing density in the doublet wavefunctions along the three nodal planes of the exchange holes for decreasing ω_z is caused by the increasingly stronger potential walls of the electron–electron interaction along these planes.

The energy spectra for a strongly anharmonic Gaussian potential have also been calculated for the same three regimes of confinement strength ω_z as for the nearly harmonic case. For strong and medium confinement the energy spectra look quite similar to those of the nearly harmonic case, while for weak confinement of $\omega_z = 0.1$ the spectrum shows an irregular level structure in the high energy region above $\Delta E > 3.0$. The nodal planes of the wavefunctions in this high energy region become curved and it becomes difficult to assign these wavefunctions by counting the number of nodal lines for the three normal modes, suggesting a transition from the normal modes to other localized modes.

Acknowledgments

The present study has been supported in part by Grants-in-Aid for Scientific Research (No 18750018) from the Ministry of Education, Science, Sports and Culture and by a fund from the Matsuo Foundation. TS thanks the Alexander von Humboldt Foundation for a resumption of his fellowship.

References

[1] Murray C B, Norris D J and Bawendi M G 1993 *J. Am. Chem. Soc.* **115** 8706–15
[2] Ashoori R C 1996 *Nature* **379** 413–9
[3] Tarucha S, Austing D G, Honda T, van der Hage R T and Kouwenhoven L P 1996 *Phys. Rev. Lett.* **77** 3613–6
[4] Johnson N F 1995 *J. Phys.: Condens. Matter* **7** 965–89
[5] Klimov V I, Mikhailovsky A A, Xu Su, Malko A, Hollingsworth J A, Leatherdale C A, Eisler H-J and Bawendi M G 1996 *Science* **290** 314–7
[6] Pavesi L, Dal Negro L, Mazzoleni C, Franzó G and Priolo F 2000 *Nature* **408** 440–3
[7] Biolatti E, Iotti R C, Zanardi P and Rossi F 2000 *Phys. Rev. Lett.* **85** 5647–50
[8] Loss D and DiVincenzo D P 1998 *Phys. Rev.* A **57** 120–6
[9] Alivisatos A P 1996 *Science* **271** 933–7
[10] Ezaki T, Mori N and Hamaguchi C 1997 *Phys. Rev.* B **56** 6428–31
[11] Cantele G, Ninno D and Iadonisi G 2001 *Phys. Rev.* B **64** 125325
[12] Hu J, Odom T W and Lieber C M 1999 *Acc. Chem. Res.* **32** 435–45
[13] Rontani M, Rossi F, Manghi F and Molinari E 1999 *Phys. Rev.* B **59** 10165–75
[14] Bryant G W 1987 *Phys. Rev. Lett.* **59** 1140–3
[15] Merkt U, Huser J and Wagner M 1991 *Phys. Rev.* B **43** 7320–3
[16] Sako T and Diercksen G H F 2003 *J. Phys. B: At. Mol. Opt. Phys.* **36** 1433–57
[17] Sako T and Diercksen G H F 2003 *J. Phys.: Condens. Matter* **15** 5487–509
[18] Sako T and Diercksen G H F 2005 *J. Phys.: Condens. Matter* **17** 5159–78
[19] Szafran B, Adamowski J and Bednarek S 2000 *Physica* E **5** 185–95
[20] Wigner E 1934 *Phys. Rev.* **46** 1002–11
[21] Sako T and Diercksen G H F 2007 *Phys. Rev.* B **75** 115413
[22] Chui S T 1986 *Phys. Rev. Lett.* **56** 2395–8
[23] Häusler W and Kramer B 1993 *Phys. Rev.* B **47** 16353–7
[24] Sako T, Hervieux P A and Diercksen G H F 2006 *Phys. Rev.* B **74** 045329
[25] Maksym P A and Chakraborty T 1990 *Phys. Rev. Lett.* **65** 108–11
[26] Matagne P and Leburton J P 2002 *Phys. Rev.* B **65** 235323
[27] Wagner M, Merkt U and Chaplik A V 1992 *Phys. Rev.* B **45** 1951–4

[28] Lin J T and Jiang T F 2001 *Phys. Rev.* B **64** 195323
[29] Dippel O, Schmelcher P and Cederbaum L S 1994 *Phys. Rev.* A **49** 4415–29
[30] Becken W, Schmelcher P and Diakonos F K 1999 *J. Phys. B: At. Mol. Opt. Phys.* **32** 1557–84
[31] Drouvelis P S, Schmelcher P and Diakonos F K 2004 *J. Phys.: Condens. Matter* **16** 3633–46
[32] Drouvelis P S, Schmelcher P and Diakonos F K 2004 *Phys. Rev.* B **69** 035333
[33] Braskén M, Lindberg M, Sundholm D and Olsen J 2000 *Phys. Rev.* B **61** 7652–5
[34] Corni S, Braskén M, Lindberg M, Olsen J and Sundholm D 2003 *Phys. Rev.* B **67** 085314
[35] Szafran B, Peeters F M, Bednarek S, Chwiej T and Adamowski J 2004 *Phys. Rev.* B **70** 035401
[36] Kohn W 1961 *Phys. Rev.* **123** 1242–4
[37] Brey L, Johnson N F and Halperin B I 1989 *Phys. Rev.* B **40** 10647–9
[38] Peeters F M 1990 *Phys. Rev.* B **42** 1486–7
[39] Li Q P, Karraï K, Yip S K, Das S S and Drew H D 1991 *Phys. Rev.* B **43** 5151–4
[40] Dobson J F 1994 *Phys. Rev. Lett.* **73** 2244–7
[41] Pi M, Ancilotto F, Lipparini E and Mayol R 2004 *Physica* E **24** 297–307
[42] Duch W and Karwowski J 1985 *Comput. Phys. Rep.* **2** 93–170
[43] Kotani M, Amemiya A, Ishiguro E and Kimura T 1955 *Table of Molecular Integrals* (Tokyo: Maruzen)
[44] Sako T and Diercksen G H F 2008 in preparation
[45] Sako T, Aoki D, Yamanouchi K and Iachello F 2000 *J. Chem. Phys.* **113** 6063–9